A methodology to reach high power factor during multiple EV charging sessions

Regina Lamedica[a], Marco Maccioni[a], Alessandro Ruvio[a, *], Tudor Gabriel Timar[a], Federico Carere[a], Eleonora Sammartino[b], Diego Ferrazza[b]

[a] Dept. of Astronautics, Electrical and Energy Engineering (DIAEE), "Sapienza" University of Rome, Rome, Italy

[b] Enel X S.r.l., Rome, Italy

Acronyms

AC	Alternating Current
DC	Direct Current
DN	Distribution Network
EV	Electric Vehicle
G2V	Grid to Vehicle
LV	Low Voltage
MV	Medium Voltage
PF	Power Factor
PFC	Power Factor Correction
POD	Point of Delivery
SOC	State of Charge
SS	Secondary Substation
V2G	Vehicle to Grid

Variables

V_1	RMS value of the first harmonic of the voltage
I_1	RMS value of the first harmonic of the current
φ_1	Phase difference between V_1 and I_1
PF_{System}	PF calculated at the POD
SOC_{th}	Threshold value of SOC

*Corresponding author. Tel.: +390644558521.
E-mail address: alessandro.ruvio@uniroma1.it (Alessandro Ruvio).

PF_{lim}	Threshold value of PF under which the algorithm is activated
PF_{mem}	PF value considering the system without the last stand-by decision
EV_{numSOC}	Number of EVs with a SOC greater than the threshold value
PF_{min}	Minimum PF in the time period analysis
T	PF violation percentage
N_T	Total number of timestamps of the simulation

Abstract

The paper suggests a new methodology to increase the PF of a hub for EV charging. A smart management of the EV charging sessions allows to impose the stand-by operation of a vehicle based on the local PF value at EV charging points. Current harmonics are taken into account to ensure an effective improvement of the hub power quality. The case study of this paper consists of a hub for EV charging with a dedicated MV/LV substation, enriched by an experimental dataset containing measurements of 13 EVs during charging in terms of active and reactive power profiles, current harmonics, PF trends. The model is developed in Simulink environment and the proposed algorithm is implemented in a MATLAB script. The results highlight that in case of multiple EV charging sessions, the algorithm is able to maintain the hub PF value greater than the acceptable PF threshold limit. This scenario is expectable in real conditions, e.g. EV hubs near shopping centres or in cities with high population density.

Keywords: Algorithm; electric vehicles; charging; power factor; power quality

1 Introduction

The widespread increase of EV sales requires a massive infrastructure upgrade, both of power and number of EV charging stations and of the DN. According to Deloitte global forecast, total EV sales will achieve 11.2 million in 2025, then reaching 31.1 million by 2030. EVs would secure approximately 32% of the total market share for new car sales [1]. Power grid challenges (e.g. reliability, greenhouse gas and carbon emissions, economics, safety, energy security) require a new,

flexible and more complex grid, the so-called smart grid. National Institute of Standards and Technology chose to focus on seven key functionalities plus cybersecurity and network communications; one of those is electric transportation [2]. The penetration of EV charging stations in the DN forces to upgrade the MV grid and to analyse carefully the LV grids which directly supply the charging stations.

The power quality decrease due to EV penetration is deeply analysed in literature [3-6]. The authors point out that the main consequences of EV charging sessions are high harmonics levels and voltage deviations, power losses, transformer overloading. In [3], the main power quality issues caused by fast EV charging stations are summarized in the following: voltage fluctuation, harmonic stability, harmonic emission. Reference [4] states that the quick charging rate causes significant voltage harmonics and power losses; moreover, for high penetration degrees, as in affluent neighbourhoods, EVs will cause unacceptable and severe voltage harmonics, deviations, power losses and transformer overloading, thus stressing the LV grids. In [5], the authors analyse the V2G and G2V technologies as solutions for power quality issues, highlighting the costs of this type of solution (e.g. battery degradation, need for intensive communication between the vehicles and the grid, effects on grid distribution equipment, infrastructure changes and social, political, cultural, and technical obstacles). In [6], the authors suggest a new mixed deterministic and probabilistic method in order to reach high levels of power quality, thanks to a pre-evaluation of harmonic disturbance.

A review of the main power quality issues due to EVs and the main remedial actions are illustrated in [7]. In detail, the so-called PQ problems (e.g. voltage sag, interruptions, harmonics presence) are analysed considering the widespread penetration of power electronic devices, as the converters for EV chargers [8-9]. Under this regard, [9] proposes an algorithm able to manage and control the EV charging in a parking area, with the aim to keep the total harmonic distortion under a fixed threshold limit.

The necessity to maintain the PF as near as possible to 1 is a crucial aspect to investigate and it is stressed by a relevant number of studies; nonetheless, the suggested solutions in literature mostly propose adjustments or new designs of the electronic devices.

A strategy to maintain high PF values consists of implementing a PF correction control mechanism on the on-board conversion system, as investigated in [10-16]. In [10], the authors propose a boost inverter-based single stage EV charger and a DC-side capacitor able to supply reactive power compensation and limiting the ripple current; in [11], a single-stage on-board battery charger for EV and plug-in hybrid EV applications is presented for PFC; in [12] the PFC is performed by means of an improved power quality Cuk converter-fed isolated LLC resonant converter for an EV battery charger, while in [13] by means of a single-phase on-board charger; in [14], a new front end ac–dc bridgeless interleaved PFC topology is proposed for level II plug-in hybrid EV battery charging; in [15], a modified PFC ON/OFF control and 3D printed circuit board design for a high-efficiency and high-power density is investigated; in [16], the authors suggest a nonlinear sliding-mode controller for a three-phase converter, employed in plug-in EVs onboard charger. According to these studies, the optimal management of the power exchanged with the LV grid can be obtained independently for each EV.

Other studies investigate the EVs capabilities to provide ancillary services for the distribution grid, focusing on specific requirements. The V2G and G2V mechanisms are often suggested to provide voltage support and reactive compensation [17-18]. In [17], a distributed model predictive control strategy is implemented to improve the real-time DN voltage regulation, both for balanced and unbalanced distribution networks. The authors stress the importance to propose suitable strategies also in case of irregular user integration and relatively poor communication infrastructure. In literature, the V2G technology is also used to allow renewables power plant penetration, as in [19-20], where the cost reduction is achieved by coordinating renewable generation with EV charging and discharging sessions, also providing ancillary services to the grid. The feasibility of the ancillary

services for EV managers is investigated in literature, taking into account cost-benefit analysis. In [21], the authors consider a battery degradation cost to ensure the active participation in V2G energy exchanges for final users and EV aggregators. Other papers suggest an optimization framework in which the look-ahead power demand of the vehicles is analysed [22-23].

Few papers analyse the PFC as an ancillary service for the grid without focusing on the on-board converter design. In [24], an improved control strategy for PF correction is proposed in case of a three-phase microgrid composed of a PV array, dynamic loads, and an EV parking lot. The control system manages the EV charging sessions trying to schedule the EV power request during PV generation surplus. In order to correct the PF at the POD, the system can require some EV chargers to limit the active power absorption with the aim to inject reactive power, thus decreasing the charging process, or to provide reactive compensation by injecting only reactive power. Nevertheless, the harmonic distortion is not simulated, the electrical grid is simplified and the simulations do not exploit real EV data. In [25], the authors highlighted that EV control systems are influenced by the harmonic distortion, mainly evident in currents. In [26], the EV charging starting times are scheduled in order to mitigate voltage deviations in residential LV distribution systems. A detailed representation of the LV grid supplying the charging hub is proposed but, also in this case, the harmonic distortion is not considered and the PFC is not the main target.

This paper proposes a new algorithm able to mitigate the PF decrease at the POD of an EV charging hub, forcing EVs with a low PF to a stand-by operation. The model exploits an experimental dataset obtained in different EV charging sessions: a detailed implementation in Simulink environment has been carried out and validated against experimental measurements. The proposed algorithm could be implemented in real environments with a new flexible energy market, in which the aggregator plays a fundamental role [27].

The main contributions of this paper to the literature are summarized in the following list:

- Experimental data of 13 EVs are provided by Enel X to test the PF and the power quality of a charging hub.
- This paper suggests a PF correction algorithm for an EVs fast-charging hub, considering both AC and DC connections.
- A detailed three-phase representation of the EV charging hub is proposed, incorporating harmonic disturbances, detailed models of the LV distribution grid and the MV/LV transformer, metering infrastructure features.

The paper is organised as follows. Section 2 describes the currently adopted standardization of EV charging stations and Section 3 illustrates the implemented model of the EV charging hub, including metering infrastructure and harmonic disturbances. Section 4 illustrates the proposed PFC algorithm; Section 5 presents the case study. Results are reported in Section 6, which also discusses the feasibility of the algorithm; lastly, Section 7 concludes the paper.

2 EV Charging Stations features

IEC 61851 standardizes four charging modes [4]. The first three modes perform ac charging with on-board charger, whereas mode 4 presents a dc charging and an off-board charger. The main details are reported below:

1. Mode 1 is a slow ac charging from a household-type socket outlet; the voltage is up to 250 V single-phase or 480 V three-phase and the current is up to 16 A.
2. Mode 2 is a slow ac charging from a household-type socket outlet with an in-cable protection device; the voltage is limited to 250 V single-phase or 480 V three-phase and the current is limited to 32 A.
3. Mode 3 performs both fast and slow ac charging using a specific EV socket outlet with control and protection function installed.

4. Mode 4 is a fast dc charging; utilizing a DC EV supply equipment with a control pilot function that extends from the DC EV supply equipment to the EV.

Three power supply categories are defined:

1. 3.7 kW (slow charging—normal power): mainly for domestic applications and long-time parking;
2. 3.7 ÷ 22 kW (quick charging—medium power): for public and private charging stations;
3. >22 kW (fast charging—high power): for public stations.

In particular, typologies of charging stations installed in the Italian DNs are:

1. public AC stations: rated power up to 22 kW
2. public AC stations: rated power 43 kW
3. private AC stations: rated power from 3.7 to 22 kW
4. fast charge: 43 kW ac rated power, 50 kW dc rated power
5. high power charge: rated power up to 350 kW dc

3 Modelling of EV charging hubs

A method able to increase the PF at the POD of a hub for EV charging is investigated and proposed. The model of the hub is implemented in the Simulink environment, including both the electrical power components and the measurement infrastructure. The library "Specialized Power Systems" in Simulink has been used [28]. The nominal power of charging stations is assumed equal to 2x22 kW in AC three-phase mode and 2x7 kW in AC single-phase mode; these charging stations are very common infrastructure in Italy. Figure 1 illustrates the Simulink model of the hub. The components used are listed below.

- SS

- LV cables (L_1 and L_2)
- 4 EVs
- Generator of harmonic currents (Harmonics EV_i)
- Metering infrastructure (M1, MEV_i)

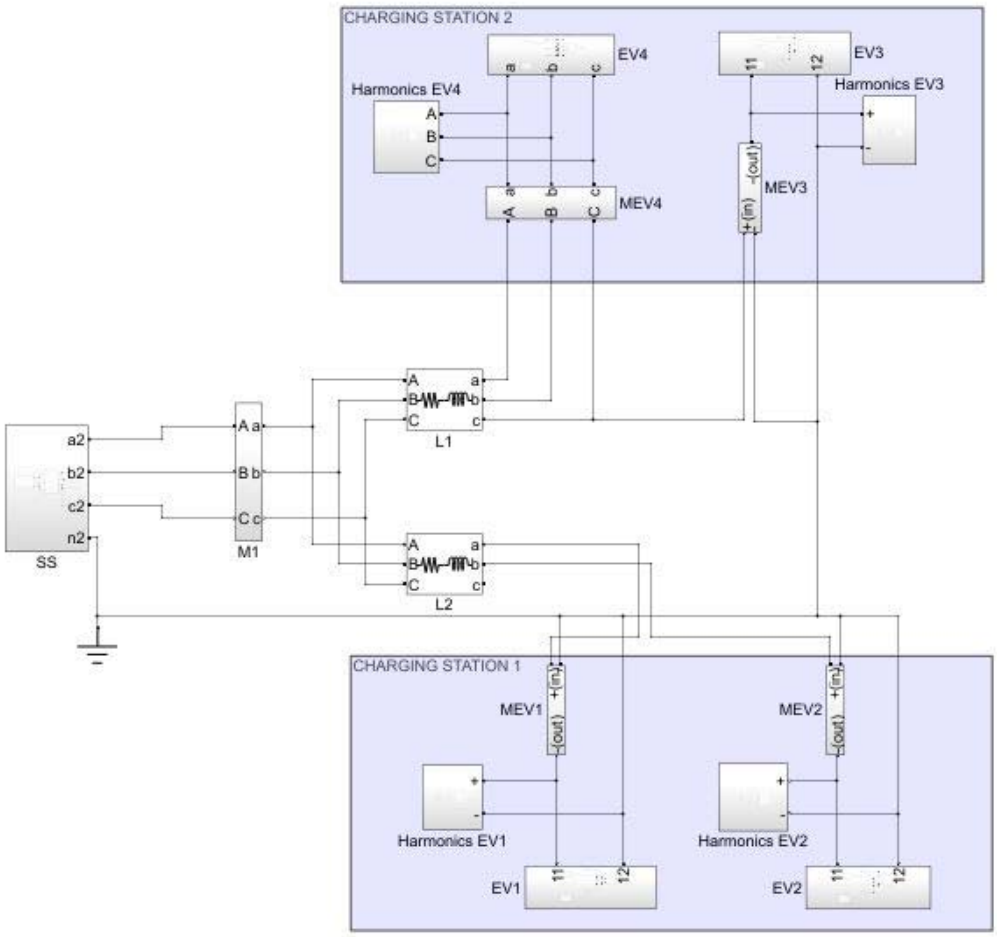

Figure 1: Simulink model of the EV charging hub implemented in Simulink

The external MV grid is considered able to supply the total requested power; the SS is modelled as a voltage generator in series with a MV/LV transformer. The voltage generator is simulated by means of the "Three-Phase Source" block, that implements a balanced three-phase voltage source with an internal R-L impedance [28]. The MV/LV transformer is simulated by means of the "Three-Phase

Transformer Inductance Matrix Type (Two Windings)" block, that models a three-phase transformer with a three-limb core and two windings per phase [28].

LV cables are modelled as RLC impedances, single or three phase according to the charging type. The "Three-Phase Series RLC Branch" block, that implements three balanced branches consisting each of a resistor, an inductor, or a capacitor, has been used [28].

The EV model is implemented considering the possibility to have a deterministic or probabilistic approach to define a dataset of EV charging sessions characterized by:

- Active and reactive profiles of the charging sessions
- RMS value of the first harmonic of the voltage, V_1
- RMS value of the first harmonic of the current, I_1,
- Phase difference φ_1 between V_1 and I_1.

The EV model is illustrated in Fig. 2 in case of a single-phase connection type. The model is based on the block "Single-Phase Dynamic Load" [28], that represents a single-phase load and is properly modified in this paper in order to modify active and reactive power consumption during time, as formulated in (1).

$$\bar{I} = \frac{P - jQ}{\sqrt{3} \cdot \bar{V}^*} \tag{1}$$

where P is the active power, Q the reactive power, $\bar{V}^*$ is the conjugate of the phase-to-ground voltage phasor. The reported equation is implemented in the subsystem "Positive sequence current" of the "Single-Phase Dynamic Load" block, entirely replacing the previous subsystem. The new subsystem is reported in Fig. 2.

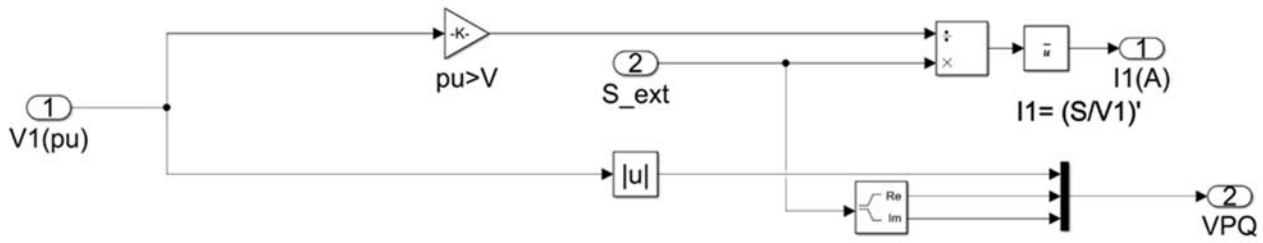

Figure 2: "Positive sequence current" subsystem of "Single-Phase Dynamic Load".

The block calculates the current according the actual active and reactive power profiles. The voltage at the point of connection of the charging station is variable, due to the influence of all other electrical components installed along the line; therefore, the current value is approximated. Another possible approximation would be the calculation of active and reactive power by using the actual value of the current (in such a way active and reactive power are approximated). The authors used the first approximation, related to the current, because the PF evaluation is performed using active and reactive power values.

Another block, named SOC, is necessary to evaluate the EV state of charge during time, as described in the following equation:

$$SOC(t) = \frac{\int_0^{\tau} p(\tau) d\tau}{E_{Batt}} \tag{2}$$

where E_{Batt} is the maximum energy stored in the EV battery and p is the active power at the timestamp τ. SOC is necessary to identify the initial operating point of the charging session.

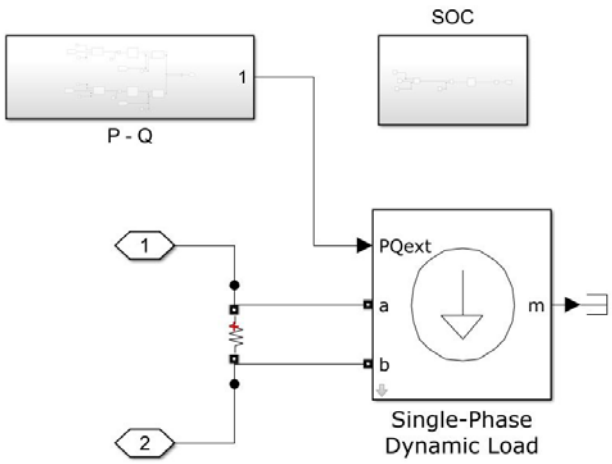

Figure 3: EV model in Simulink

Active and reactive power absorbed by the EV, simulated by the "Single-Phase Dynamic Load", must be set to zero when the PF algorithm requires the stand-by operation of the EV. After the stand-by phase, the vehicle continues the charging session from the previous operating point. Therefore, active and reactive power profiles present an inactive situation corresponding to the stand-by period. In Simulink environment, the stand-by operation effect on power profiles, described before, is realized through the "1-D Lookup Table" [28], that evaluates a sampled representation of a function. In Fig. 4, the Simulink model that generates the modified active and reactive profile of the vehicles is represented. The upper and lower parts of the model are the same, respectively for active and reactive power. In this paper, the 1-D Lookup Table block associates the timestamp of the simulation to the correspondent values of active and reactive power of the EV of the dataset. The stand-by operation is identified through the signal PWM1, a Boolean value that can assume either 1 or 0, respectively for normal and stand-by operation. The input of the 1-D block is generated integrating a constant through the "Integrator" block [29]: in such a way, the input signal of the 1-D Lookup Table block is equal to the time signal but is interrupted during the stand-by operation and restarts once the stand-by phase ends.

In case of three-phase charging, the model is very similar: the "Three-Phase Dynamic Load" block is adopted and the system is supposed symmetric and balanced.

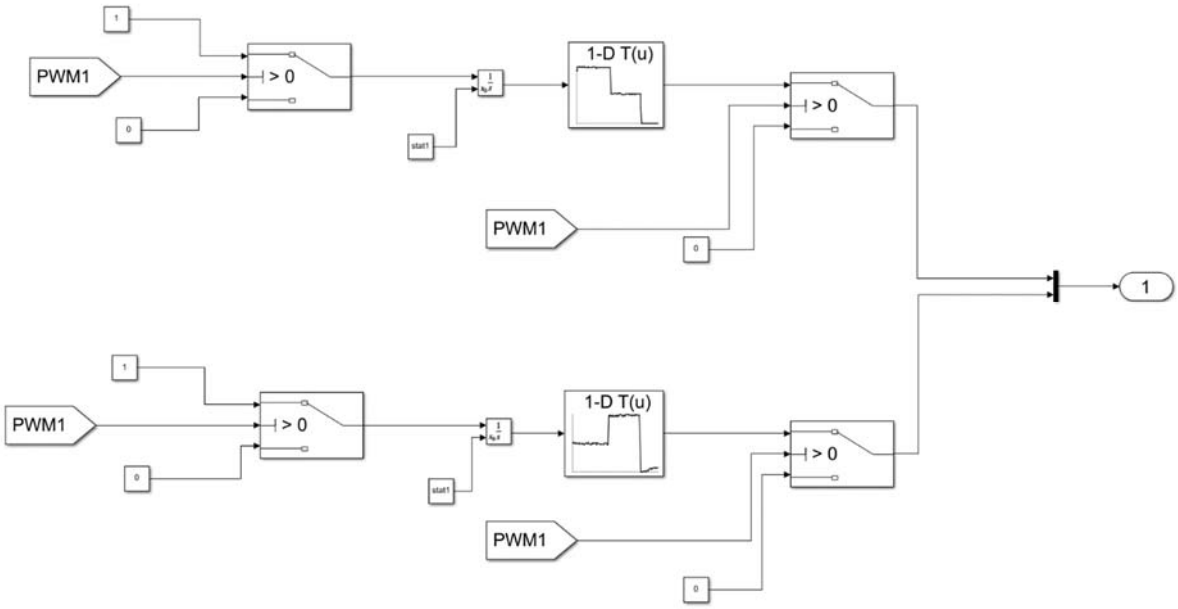

Figure 4: P-Q block of the EV model in Simulink

The current harmonics are simulated by means of a current generator injecting in the grid the following current:

$$i(t) = I_3 \sin(3\omega t + \varphi_3) + I_5 \sin(5\omega t + \varphi_5) + \cdots + I_{25} \sin(25\omega t + \varphi_{25}) \quad (3)$$

Taken into account experimental data reported in following sections, only odd harmonics have been considered, from the 3rd up to the 25th. The harmonic amplitudes during the charging phase are extracted by the measurement dataset, whereas the harmonic phase angles are randomly variated from the minimum and maximum values through a simple MATLAB script.

The metering infrastructure monitors the connection with the SS (M1) and each EV charging point (MEV_i), with different electrical connections in case of single-phase or three-phase charging. For the three-phase connection, the PF of the single phase and the PF of the three-phase system are calculated with the following:

$$S_1 = V_{1,rms} \cdot I_{rms} \quad (4)$$

$$PF = \frac{P_1}{S_1} \qquad (5)$$

$$PF_{System} = \frac{P_A + P_B + P_C}{V_{1,A,rms} \cdot I_{A,rms} + V_{1,B,rms} \cdot I_{B,rms} + V_{1,C,rms} \cdot I_{C,rms}} \qquad (6)$$

where index 1 means that the variable is calculated neglecting voltage harmonics, whereas A, B, C refer to the three phases of the system. In detail, S_1 is the apparent power related to one of the phases and calculated neglecting voltage harmonics, $V_{1,rms}$ is the rms value of voltage to ground of one of the phases without harmonics, I_{rms} is the rms value of the current of one of the phases. The other variables follow the same convention.

4 PF mitigation algorithm

The PF mitigation algorithm has been developed to increase the overall PF, PF_{System}, through the temporary interruption of the charging sessions of some EVs connected to the hub. Based on the experimental dataset, low PFs are associated with high SOC levels of the EV battery. The algorithm is illustrated in Fig. 5 and the main variables are reported in the following list:

- SOC_{th}: the threshold value of SOC;
- PF_{lim}: the threshold value of PF under which the algorithm is activated;
- PF_{mem}: the value of PF considering the system without the last stand-by decision;
- EV_{numSOC}: the number of EVs with a SOC greater than the threshold value.

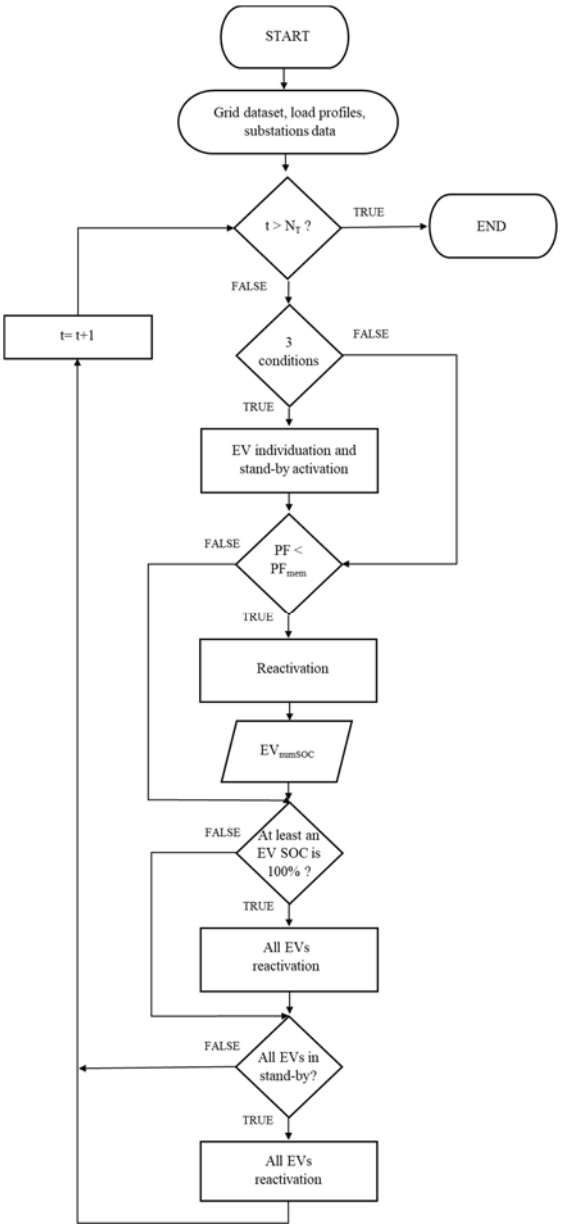

Figure 5: Flowchart of PF algorithm

The algorithm is implemented in MATLAB: initially the characteristics of the system (grid dataset, load profiles, substation data) are read and the timestamp loop starts. The three conditions that allow the stand-by of an EV are the following:

1. Almost one of the EVs has a SOC greater than SOC_{th};
2. The PF_{System} value calculated at timestamp t is lower than PF_{lim};
3. The number of EVs with a SOC greater than SOC_{th} is larger than EV_{numSOC}

The third condition is imposed because, in case of the reactivation of a charging session, the algorithm must wait for another EV to overcome the SOC_{th}, in order to avoid a useless stand-by operation with the same scenario.

If all the three conditions are met, the algorithm selects the EV with the smallest PF and with a SOC greater than SOC_{th} and puts it in stand-by. The effect on the overall PF_{System} due to the stopped charging sessions is verified, comparing the actual value to the PF_{mem}. In case of a negative impact of the operation, the EV charging session is reactivated and the EV_{numSOC} is updated. Moreover, the PF algorithm performs two checks: if the SOC of at least one EV is 100% or all EVs are in stand-by operation, then all the EVs are reactivated.

5 Case Study

The case study is an EV charging hub: experimental measurements of 13 EVs during charging have been considered. Out of the 13 EVs, 11 have a single-phase connection and 2 a three-phase connection, with a maximum current of 16 and 32 A, respectively. Charging type of all the considered EVs are reported in Table 1 in order to clarify the simulation scenario and the results.

Table 1: Charging type of EVs.

EV	**Charging type**	**I_{max} (A)**
EV_1	Single-phase	16
EV_2	Single-phase	32
EV_3	Single-phase	16
EV_4	Three-phase	16
EV_5	Single-phase	32
EV_6	Single-phase	16
EV_7	Single-phase	32
EV_8	Single-phase	16
EV_9	Single-phase	16
EV_{10}	Single-phase	32
EV_{11}	Single-phase	32
EV_{12}	Single-phase	16
EV_{13}	Three-phase	32

Active and reactive power profiles, current harmonics, PF trends are part of the dataset obtained with the experimental tests. The harmonic component was investigated modifying the charging power through a PWM technique. Table 2 reports an example of the harmonic dataset for a single-phase EV. Maximum and minimum current harmonics magnitudes, in per cent of the current value at the fundamental frequency, are provided by experimental tests, whereas maximum and minimum phase angles of current harmonics are randomly generated in a defined range through a MATLAB script.

Table 2: Example of current harmonics dataset for a single-phase EV.

Harmonic order	**Minimum Magnitude (%)**	**Maximum Magnitude (%)**	**Minimum Phase Angle**	**Maximum Phase Angle**
3	5.71	16.43	-20	20
5	1.43	8.14	-20	20
7	2.86	5.50	-20	20
9	2.14	2.86	-20	20
11	1.43	2.36	-20	20
13	0.71	1.50	-20	20
15	0.36	1.07	-20	20
17	0.43	0.93	-20	20
19	0.43	0.79	-20	20
21	0.50	0.71	-20	20
23	0.43	0.64	-20	20
25	0.29	0.64	-20	20

Table 3 reports the main electrical characteristics of the MV/LV transformer installed in the SS which the hub is connected to.

Table 3: Main electrical characteristics of the MV/LV transformer installed in the SS.

Primary/Secondary voltage	**Power (kVA)**	**Pcc (%)**	**P_0 (%)**	**Vcc (%)**	**I_0 (%)**
8.4/0.4	400	1.2	0.3	6	1.5

LV cables are simulated as a resistance and inductance connected in series, respectively of about $1.01 \cdot 10^{-1}$ Ω and $1.01 \cdot 10^{-4}$ H.

Two scenarios are considered in order to distinguish between a low and a high number of charging sessions in the analysed time period, respectively named low level scenario and high level scenario. A cluster of 8 EVs is examined, with their SOCs randomly selected at the beginning of the simulation.

In the low level scenario, no EV can recharge other than the ones connected to the hub at the beginning of the simulation, whereas in the high level scenario other EVs can randomly start recharging during the simulation, with a total maximum number of EVs in charge equal to 8.

Initial SOCs, number and profiles of EVs, as well as the starting time of the charging sessions vary randomly during the simulations. PF_{lim} is fixed at 0.98.

6 Results and discussion

The benefits of the PF algorithm are evaluated in the case study through a series of simulations in Simulink environment. The parameters of the simulations are the initial SOCs, the number and power profiles of EVs and the start of the charging sessions. With the aim to test the algorithm performance in different conditions, 50 simulations are carried out for both the scenarios. Simulations are initially carried out without using the proposed PF algorithm and are repeated with the activation of the PF algorithm.

The benefits derived by the application of the algorithm are evaluated through two quantities: PF_{min}, the minimum PF, and T, the number of time periods in which the PF is lower than PF_{lim} (0.98) in per cent of the overall number of time periods.

6.1 Low level scenario of EV charging sessions

The PF algorithm is tested in the low level scenario performing 50 different simulations. An example that shows how the PF algorithm operates is illustrated in Fig. 6, which reports the PF trend over time in one of the 50 simulations.

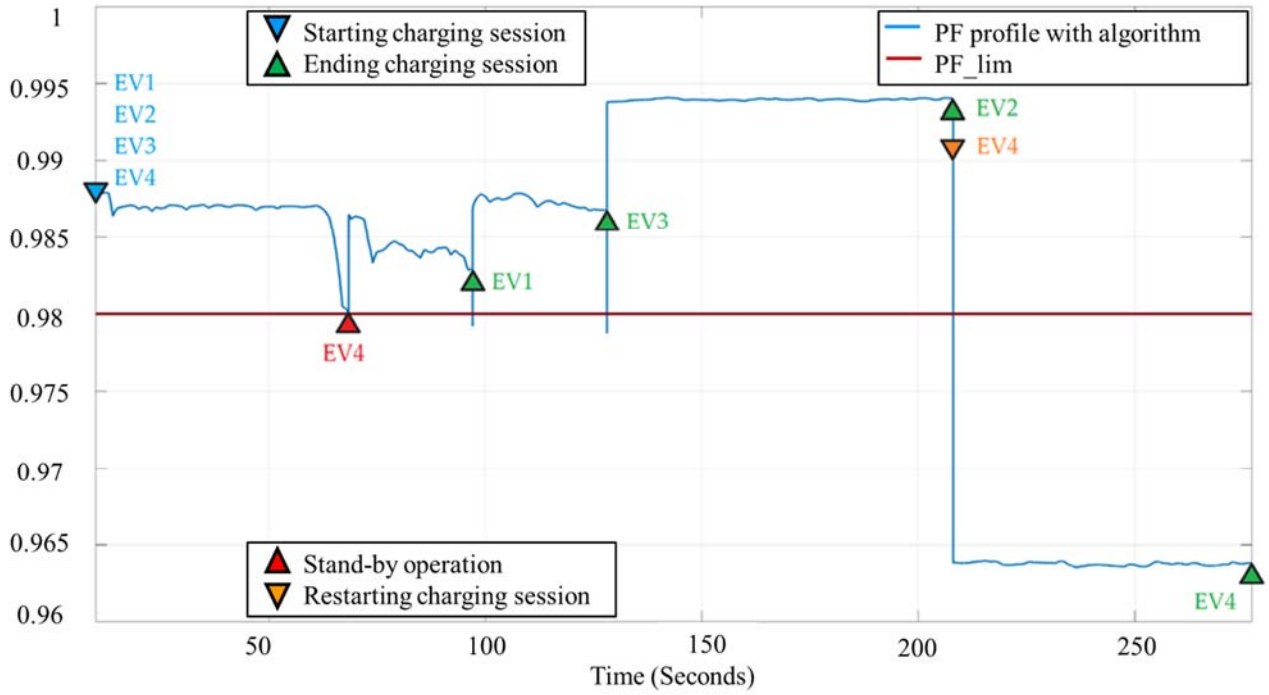

Figure 6: PF trend over time in case of algorithm operation in a selected simulation of the low level scenario.

Four EVs start charging sessions at the beginning of the simulation: the PF of the system is higher than the 0.98 threshold value (highlighted with a red line). The charging sessions of the 4 EVs proceed in the simulation without any significant PF decrease until 68 seconds after the beginning of the simulation. SOC and PF values of each EV at t=68 s are reported in Table 4.

Table 4: SOC and PF values of each EV at t=68 s.

EV ID	1	2	3	4
SOC	90.46	67.55	79.04	80.08
PF	0.977	0.996	0.975	0.963

The PF of the system is under the 0.98 threshold limit and therefore the PF algorithm is activated. EV4 is identified as the EV with the lowest PF and thus EV4 charging session is stopped: the PF of the system consequently increases, achieving a value greater than the threshold limit. The EV4 charging session is reactivated by the algorithm when another EV ends the charging session, as in the

case of EV1 and EV3, respectively at t=95 s and t=130 s, but is immediately stopped because the reactivation causes a PF value under the threshold limit. At t=208 s all EVs except EV4 have ended the charging sessions: at this timestamp the PF algorithm re-activates EV4 charging session and the PF value decreases to 0.964. EV4 is the only EV in charging mode: in this case the PF algorithm cannot interrupt the EV4 charging session and the PF value cannot exceed PF_{lim}. The simulation ends at t=280 s when the EV4 charging session ends. Considering the whole simulation, the calculated T value is 27.81%.

The above-described simulation highlights how the PF algorithm is not adequate in case the number of simultaneous EV charging sessions is low, as in the low level scenario. The results of the 50 simulations confirm that the algorithm cannot improve the PF profile of the system. Figures 7 and 8 show the results of all the simulations, respectively comparing the values of T and of the system PF obtained in case the PF algorithm is executed or not.

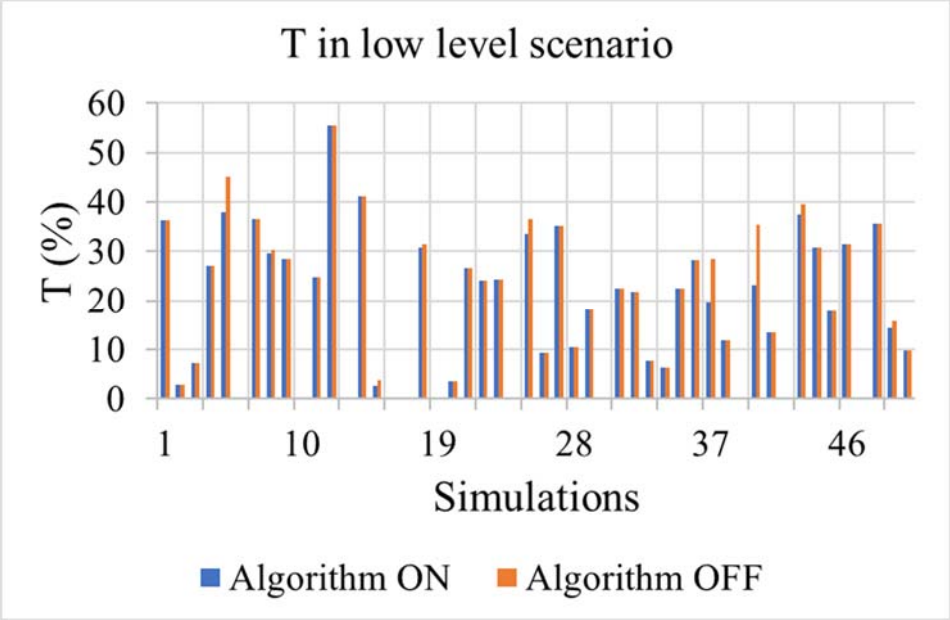

Figure 7: Overall T values in the low level scenario. Blue bars: PF algorithm is applied; orange bars: PF algorithm is not applied.

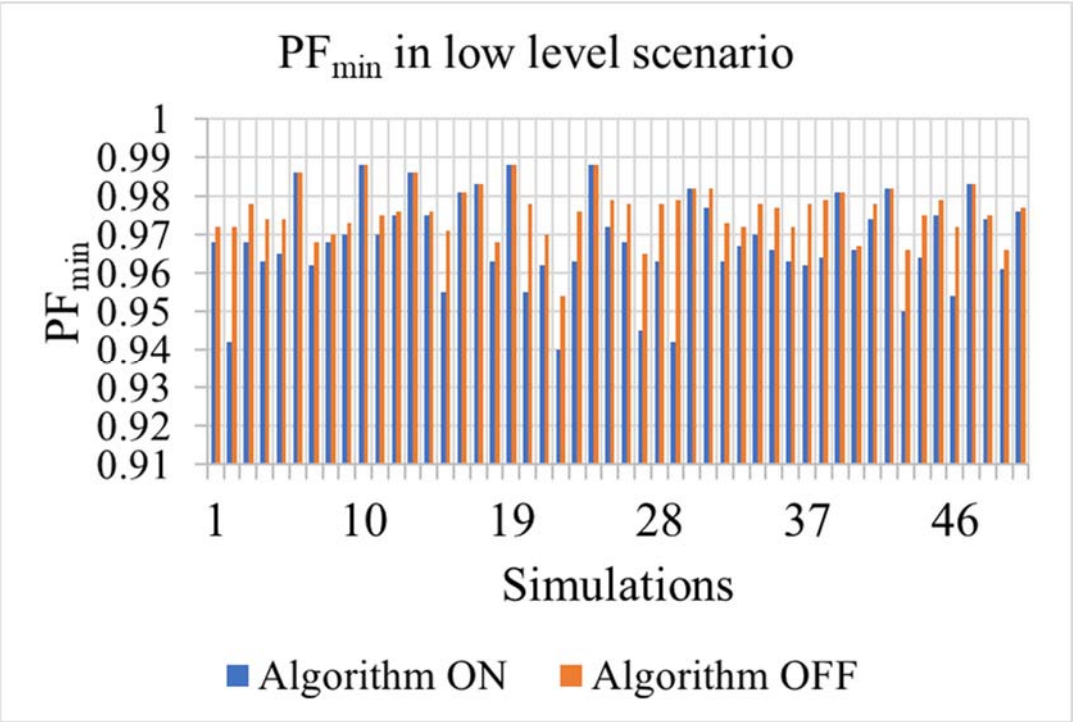

Figure 8: Overall PF_{min} values in the low level scenario. Blue bars: PF algorithm is applied; orange bars: PF algorithm is not applied.

As shown in Fig. 7, the reduction of T provided by the algorithm is often negligible and only in three out of fifty cases is larger than 5% with respect to the case that the algorithm is off; moreover, Fig. 8 also shows that in many cases the minimum PF obtained in the simulations is lower when the algorithm is on.

6.2 High level scenario of EV charging sessions

In the high level scenario, the number of EVs in charging mode is increased and the charging sessions can randomly start also after the beginning of each simulation. Figure 9 reports an example to illustrate the PF algorithm operation in the high level scenario: the simulation is very similar to the one in Fig. 6 of the previous section, with the aim to show that the number of EVs simultaneously in charge is a crucial aspect for the effectiveness of the PF algorithm. At the beginning, the hub configuration is the same of Fig. 6, with four EVs in charging, but in this case at t=202 s EV5 starts charging, thus decreasing the system PF in the time period 202÷208 s. At 208 s, EV2 ends charging

but EV5 is still charging, so the PF algorithm re-activates the EV4 charging session. In this scenario, the system PF does not decrease under the 0.98 threshold limit.

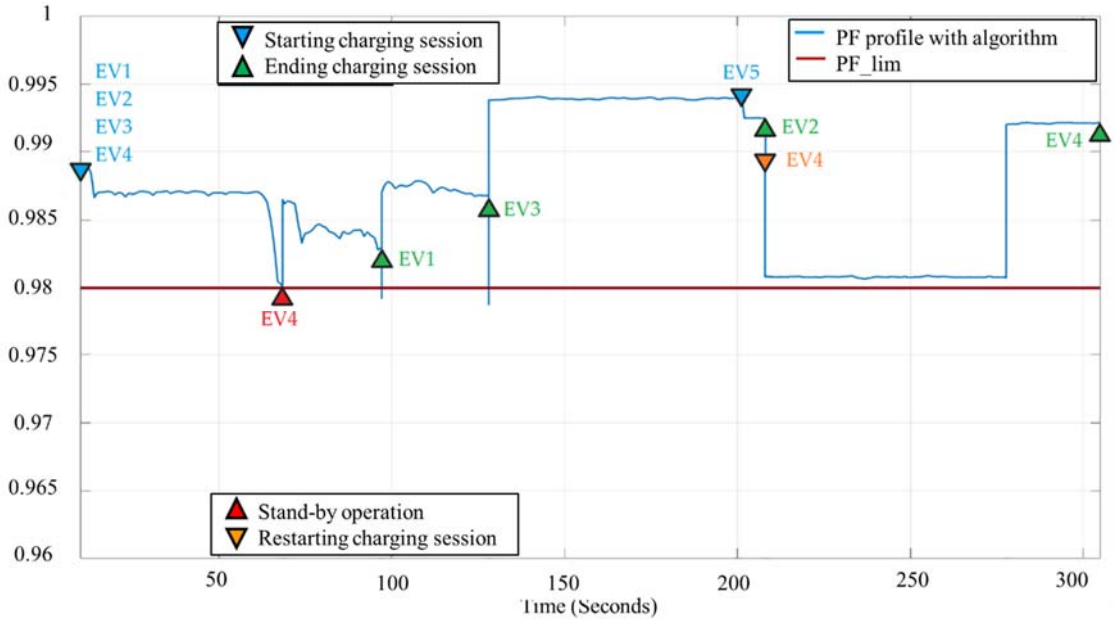

Figure 9: PF trend over time in case of algorithm operation in a selected simulation of the high level scenario.

As previously discussed, the presence of a larger number of EVs in charging mode facilitate the operation of PF algorithm. Results of the 50 random simulations confirm this aspect, as highlighted by Figs. 10 and 11.

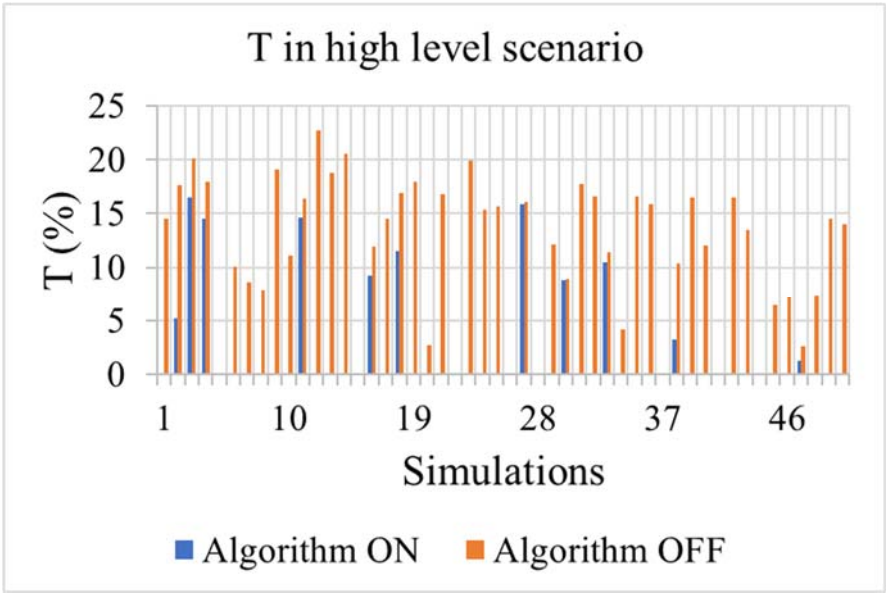

Figure 10: Overall T values in the high level scenario. Blue bars: PF algorithm is applied; orange bars: PF algorithm is not applied.

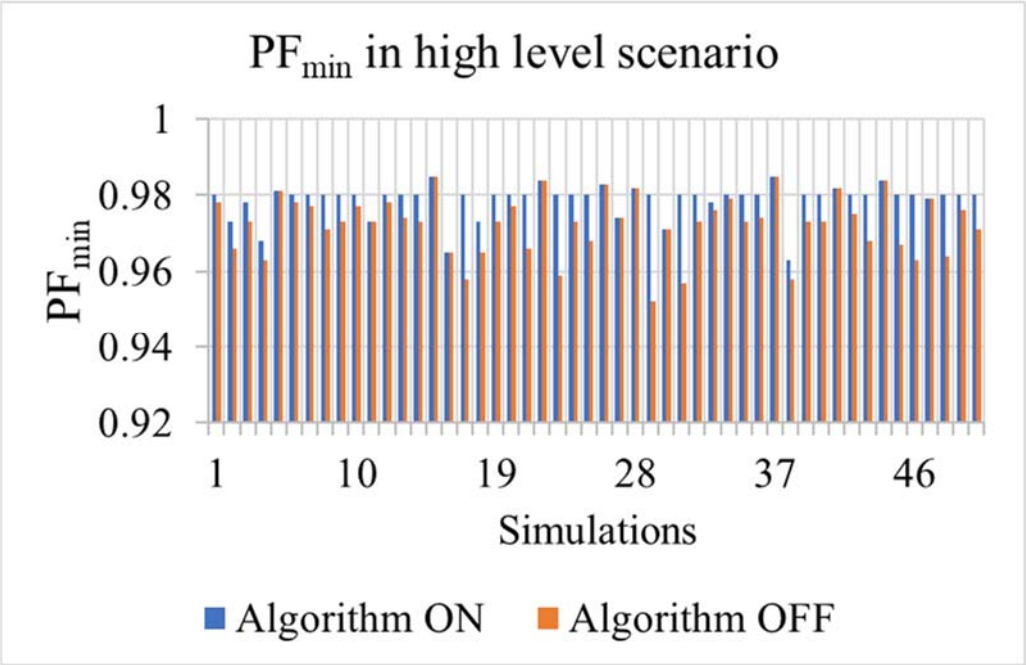

Figure 11: Overall PF_{min} values in the high level scenario. Blue bars: PF algorithm is applied; orange bars: PF algorithm is not applied.

Overall, the average reduction of T obtained by the application of the PF algorithm is 67.6%; if the cases in which the PF algorithm cannot be activated (i.e., the three conditions in Section 4 are not met) are excluded, the average reduction reaches 80.4%. In most of the simulations the application of the PF algorithm yields a PF_{min} value greater of equal than PF_{lim}. In general, simulations results obtained in the high level scenario clearly indicate the effectiveness of the PF algorithm in case a relevant number of EVs is simultaneously in charging mode.

7 Conclusions

A new methodology to increase the PF of an EV charging hub is discussed, and a PF algorithm able to manage the charging sessions of EVs is developed in order to obtain a better PF profile. The individuation of the EV with a high SOC and the lowest PF has proved to be a suitable way to increase the PF of the overall system. The case study of a hub for EV charging is reported in the paper and

real EVs data obtained from experimental tests are used. Results show that the increase of PF is possible in case of multiple contemporary charging sessions. This scenario is expectable in real conditions, e.g. EV hubs near shopping centres or in cities with high population density. In case a small number of EVs are contemporarily charging in the hub, PF correction may be harder to perform and the PF algorithm application could not ensure a suitable PF value during the charging sessions. The proposed PF algorithm is applicable also for DC charging mode, considering the harmonic disturbances related to the off-board converter. The authors will exploit the results of this paper to investigate the possibility to implement more complex techniques to increase the PF (e.g. PWM modulation), avoiding a relevant number of charging session interruptions.

References

[1] Deloitte “Electric vehicles - Setting a course for 2030”, available online at: https://www2.deloitte.com/uk/en/insights/focus/future-of-mobility/electric-vehicle-trends-2030.html

[2] "Advanced Metering Infrastructure in Smart Grid: Requirements, Challenges, Architectures, technologies, and Optimizations," in Smart Grids: Emerging Technologies, Challenges and Future Directions, Nova Science Publishers, 2017.

[3] L. Wang, Z. Qin, T. Slangen, P. Bauer and T. van Wijk, "Grid Impact of Electric Vehicle Fast Charging Stations: Trends, Standards, Issues and Mitigation Measures - An Overview," in IEEE Open Journal of Power Electronics, vol. 2, pp. 56-74, 2021, doi: 10.1109/OJPEL.2021.3054601.

[4] P. S. Moses, S. Deilami, A. S. Masoum and M. A. S. Masoum, "Power quality of smart grids with Plug-in Electric Vehicles considering battery charging profile," 2010 IEEE PES Innovative Smart Grid Technologies Conference Europe (ISGT Europe), 2010, pp. 1-7, doi: 10.1109/ISGTEUROPE.2010.5638983.

[5] M. Yilmaz and P. T. Krein, "Review of the Impact of Vehicle-to-Grid Technologies on Distribution Systems and Utility Interfaces," in IEEE Transactions on Power Electronics, vol. 28, no. 12, pp. 5673-5689, Dec. 2013, doi: 10.1109/TPEL.2012.2227500.

[6] R. Lamedica et al., "Integrating Electric Vehicles in Microgrids: Overview on Hosting Capacity and New Controls," in IEEE Transactions on Industry Applications, vol. 55, no. 6, pp. 7338-7346, Nov.-Dec. 2019, doi: 10.1109/TIA.2019.2933800.

[7] Ahmadi, A., Tavakoli, A., Jamborsalamati, P., Rezaei, N., Miveh, M.R., Gandoman, F.H., Heidari, A. and Nezhad, A.E. (2019), Power quality improvement in smart grids using electric vehicles: a review. IET Electr. Syst. Transp., 9: 53-64. https://doi.org/10.1049/iet-est.2018.5023.

[8] F. M. Gatta at al., "PQ and hosting capacity issues for EV charging systems penetration in real MV/LV networks," 2016 Power Systems Computation Conference (PSCC), 2016, pp. 1-7, doi: 10.1109/PSCC.2016.7540919.

[9] R. Lamedica at al., "EVs recharging management to maintain high PQ levels in LV islanded networks," 2018 18th International Conference on Harmonics and Quality of Power (ICHQP), 2018, pp. 1-6, doi: 10.1109/ICHQP.2018.8378923.

[10] D. B. Wickramasinghe Abeywardana et al., "Single-Phase Boost Inverter-Based Electric Vehicle Charger With Integrated Vehicle to Grid Reactive Power Compensation," in IEEE Transactions on Power Electronics, vol. 33, no. 4, pp. 3462-3471, April 2018, doi: 10.1109/TPEL.2017.2700944.

[11] S. Li, J. Deng and C. C. Mi, "Single-Stage Resonant Battery Charger With Inherent Power Factor Correction for Electric Vehicles," in IEEE Transactions on Vehicular Technology, vol. 62, no. 9, pp. 4336-4344, Nov. 2013, doi: 10.1109/TVT.2013.2265704.

[12] R. Pandey and B. Singh, "A Power-Factor-Corrected LLC Resonant Converter for Electric Vehicle Charger Using Cuk Converter," in IEEE Transactions on Industry Applications, vol. 55, no. 6, pp. 6278-6286, Nov.-Dec. 2019, doi: 10.1109/TIA.2019.2934059.

[13] C. Saber, D. Labrousse, B. Revol and A. Gascher, "Challenges Facing PFC of a Single-Phase On-Board Charger for Electric Vehicles Based on a Current Source Active Rectifier Input Stage," in IEEE Transactions on Power Electronics, vol. 31, no. 9, pp. 6192-6202, Sept. 2016, doi: 10.1109/TPEL.2015.2500958.

[14] F. Musavi, W. Eberle and W. G. Dunford, "A High-Performance Single-Phase Bridgeless Interleaved PFC Converter for Plug-in Hybrid Electric Vehicle Battery Chargers," in IEEE Transactions on Industry Applications, vol. 47, no. 4, pp. 1833-1843, July-Aug. 2011, doi: 10.1109/TIA.2011.2156753.

[15] Baek, J.; Park, M.-H.; Kim, T.; Youn, H.-S. Modified Power Factor Correction (PFC) Control and Printed Circuit Board (PCB) Design for High-Efficiency and High-Power Density On-Board Charger. Energies 2021, 14, 605. https://doi.org/10.3390/en14030605.

[16] Sabzehgar, R.; Roshan, Y.M.; Fajri, P. Modeling and Control of a Multifunctional Three-Phase Converter for Bidirectional Power Flow in Plug-In Electric Vehicles. Energies 2020, 13, 2591. https://doi.org/10.3390/en13102591.

[17] J. Hu, C. Ye, Y. Ding, J. Tang and S. Liu, "A Distributed MPC to Exploit Reactive Power V2G for Real-Time Voltage Regulation in Distribution Networks," in IEEE Transactions on Smart Grid, vol. 13, no. 1, pp. 576-588, Jan. 2022, doi: 10.1109/TSG.2021.3109453.

[18] G. Buja, M. Bertoluzzo and C. Fontana, "Reactive Power Compensation Capabilities of V2G-Enabled Electric Vehicles," in IEEE Transactions on Power Electronics, vol. 32, no. 12, pp. 9447-9459, Dec. 2017, doi: 10.1109/TPEL.2017.2658686.

[19] M. Falahi, H. Chou, M. Ehsani, L. Xie and K. L. Butler-Purry, "Potential Power Quality Benefits of Electric Vehicles," in IEEE Transactions on Sustainable Energy, vol. 4, no. 4, pp. 1016-1023, Oct. 2013, doi: 10.1109/TSTE.2013.2263848.

[20] Claudia Antal et al., “Blockchain based decentralized local energy flexibility market”, Energy Reports, Volume 7, 2021, Pages 5269-5288, ISSN 2352-4847, https://doi.org/10.1016/j.egyr.2021.08.118.

[21] M. Sufyan, N.A. Rahim, M.A. Muhammad, C.K. Tan, S.R.S. Raihan, A.H.A. Bakar, “Charge coordination and battery lifecycle analysis of electric vehicles with V2G implementation”, Electric Power Systems Research, Volume 184, 2020, 106307, ISSN 0378-7796, https://doi.org/10.1016/j.epsr.2020.106307.

[22] Mehdi Shamshirband, Javad Salehi, Farhad Samadi Gazijahani, “Look-ahead risk-averse power scheduling of heterogeneous electric vehicles aggregations enabling V2G and G2V systems based on information gap decision theory”, Electric Power Systems Research, Volume 173, 2019, Pages 56-70, ISSN 0378-7796, https://doi.org/10.1016/j.epsr.2019.04.018.

[23] Koukaras P. et al., “A Tri-Layer Optimization Framework for Day-Ahead Energy Scheduling Based on Cost and Discomfort Minimization”, Energies 2021, 14, 3599. https://doi.org/10.3390/en14123599.

[24] Shahab et al., Improved Control Strategy for Three-Phase Microgrid Management with Electric Vehicles Using Multi Objective Optimization Algorithm. Energies 2021, 14, 1146. https://doi.org/10.3390/en14041146.

[25] R. Lamedica et al., "Harmonic Disturbance Control in Islanded Smart Grids," 2018 International Symposium on Power Electronics, Electrical Drives, Automation and Motion (SPEEDAM), 2018, pp. 650-655, doi: 10.1109/SPEEDAM.2018.8445230.

[26] A. Dubey and S. Santoso, "Electric Vehicle Charging on Residential Distribution Systems: Impacts and Mitigations," in IEEE Access, vol. 3, pp. 1871-1893, 2015, doi: 10.1109/ACCESS.2015.2476996.

[27] F. Carere et al., "Flexibility - enabling technologies using electric vehicles," 2020 IEEE International Conference on Environment and Electrical Engineering and 2020 IEEE Industrial and Commercial Power Systems Europe (EEEIC / I&CPS Europe), 2020, pp. 1-6, doi: 10.1109/EEEIC/ICPSEurope49358.2020.9160781.

[28] Simscape Electrical Library of Simulink documentation, available online at: https://it.mathworks.com/help/physmod/sps/.

[29] Integrator block documentation, available online at: https://it.mathworks.com/help/simulink/slref/integrator.html